New Journal of Physics
The open-access journal for physics

The stochastic dance of circling sperm cells: sperm chemotaxis in the plane

B M Friedrich[1] **and F Jülicher**[1]
Max Planck Institute for the Physics of Complex Systems,
Nöthnitzer Strasse 38, 01187 Dresden, Germany
E-mail: ben@pks.mpg.de and julicher@pks.mpg.de

New Journal of Physics **10** (2008) 123025 (19pp)
Received 22 September 2008
Published 18 December 2008
Online at http://www.njp.org/
doi:10.1088/1367-2630/10/12/123025

Abstract. Biological systems such as single cells must function in the presence of fluctuations. It has been shown in a two-dimensional experimental setup that sea urchin sperm cells move toward a source of chemoattractant along planar trochoidal swimming paths, i.e. drifting circles. In these experiments, a pronounced variability of the swimming paths is observed. We present a theoretical description of sperm chemotaxis in two dimensions which takes fluctuations into account. We derive a coarse-grained theory of stochastic sperm swimming paths in a concentration field of chemoattractant. Fluctuations enter as multiplicative noise in the equations for the sperm swimming path. We discuss the stochastic properties of sperm swimming and predict a concentration-dependence of the effective diffusion constant of sperm swimming which could be tested in experiments.

[1] Author to whom any correspondence should be addressed.

Contents

1. Introduction

Sperm chemotaxis plays an important role for fertilization. Sperm cells steer up a gradient of chemoattractant, which is released by the egg, a process called chemotaxis. Sperm chemotaxis is well established in marine invertebrates with external fertilization (e.g. sea urchins [1]) and has been demonstrated in mammals (e.g. humans [2]).

Sperm cells possess a single eukaryotic flagellum of about 50 μm length. Dynein motors within this flagellum drive a regular beat of the flagellum which propels the sperm cell in a liquid [3]. Chemotaxis is mediated by a signaling system, which is located within the flagellum [1]. Specific receptors in the flagellar membrane are activated upon binding chemoattractant molecules and trigger a chain of signaling events which ultimately change the intra-flagellar calcium concentration [1, 4, 5]. The calcium concentration apparently regulates the activity of the flagellar dynein motors and results in a swimming response [6]. Interestingly, sperm cells can respond to chemotactic stimuli of subpicomolar concentration [4, 5, 7].

Here, we will focus on the chemotaxis of sea urchin sperm because of the large amount of experimental data available for this system. Chemotaxis of sea urchin sperm is usually observed under experimental conditions where sperm cells swim in a shallow observation chamber under the microscope [1, 4], [8]–[11]. In this situation, sperm cells become localized near the surfaces of the chamber where they swim along planar paths. In the absence of chemoattractant, the swimming paths are circular. The curvature of their swimming paths is a direct consequence of an asymmetry of the flagellar beat [4]. The rotational sense of circular swimming is mostly counterclockwise (when viewed in a direction parallel to the inward normal of the boundary surface).

In a concentration gradient of chemoattractant, the circular swimming paths drift toward regions of higher chemoattractant concentration; the swimming paths thus resemble trochoids [1, 8, 9]. Experiments indicate that both the intra-flagellar calcium concentration

and the curvature of the swimming path exhibit characteristic periodic modulations with the frequency of circular swimming when a sperm cell swims in a chemoattractant concentration gradient [1].

The mechanism of sperm chemotaxis can be formalized as follows [12]: while swimming along an approximately circular path in a concentration gradient of chemoattractant, a sperm cell traces a concentration stimulus from the concentration field, which is periodically modulated with the frequency of circular swimming. As a result, the chemotactic signaling system shows a periodic modulation of activity and causes a periodic modulation of the curvature of the swimming path. A periodic modulation of the curvature gives rise to a swimming path which is a drifting circle, or (prolate) trochoid. The relative direction of the drift with respect to the concentration gradient depends crucially on the phase shift between the stimulus and the curvature oscillations.

Experiments on sea urchin sperm chemotaxis reveal a pronounced variability of the observed sperm swimming paths. We argue that sperm chemotaxis is subject to fluctuations of various sources: the chemotactic stimulus, which the sperm cells receives exhibits fluctuations since the binding of chemoattractant molecules to their respective receptors is a discrete process. Additionally, intrinsic fluctuations of the chemotactic signaling system and fluctuations in the activity of the motor ensemble which drive the flagellar beat are present.

In this paper, we develop a framework to systematically account for fluctuations affecting sperm chemotaxis. Note that sperm swimming is an active process which is characterized by non-equilibrium fluctuations. Starting from a physical description of sperm chemotaxis, we derive an effective stochastic equation for the centerline of sperm swimming paths which follows stochastic trochoids. Different sources of fluctuations enter as multiplicative noise in this description. Our effective description characterizes sperm chemotaxis by a superposition of a chemotactic drift and effective diffusion. We show that the chemotaxis mechanism is robust in the presence of fluctuations and we discuss chemotactic success of sperm cells toward a single source of chemoattractant. We calculate a concentration-dependence of the diffusion constant of sperm swimming circles which could be tested in future experiments.

2. Stochastic description of sperm chemotaxis in two dimensions

2.1. Dynamic equations of sperm motion

We study sperm chemotaxis in two dimensions for sperm cells swimming near a surface. We define the swimming path as the trajectory of the sperm head averaged over one cycle of the flagellar beat. This average eliminates rapid periodic movements of the head with the frequency of the flagellar beat. The planar swimming path is parameterized by time-dependent x- and y-coordinates which we denote by $r_1(t)$ and $r_2(t)$, respectively. Throughout this paper, we will represent points in the plane (r_1, r_2) as complex numbers $\underline{\mathrm{r}} = r_1 + \mathrm{i}\, r_2$; an analogous convention applies for planar vectors. This notation will simplify the calculations.

The velocity of the swimming path $\underline{\mathrm{r}}(t)$ is characterized by the speed $v = |\dot{\underline{\mathrm{r}}}|$ and the tangent $\underline{\mathrm{t}} = \dot{\underline{\mathrm{r}}}/v$, where dots denote time derivatives. The normal vector is defined as $\underline{\mathrm{n}} = \mathrm{i}\,\underline{\mathrm{t}}$. The Frenet–Serret equations in two dimensions can now be written as complex-valued differential equations

$$\dot{\underline{\mathrm{r}}} = v\,\underline{\mathrm{t}}, \quad \dot{\underline{\mathrm{t}}} = v\,\kappa\,\underline{\mathrm{n}}, \quad \dot{\underline{\mathrm{n}}} = -v\,\kappa\,\underline{\mathrm{t}}, \tag{2.1}$$

where $\kappa = \underline{\dot{t}}\,\underline{n}^*/v$ is the (signed) curvature of the swimming path and the star denotes the complex conjugate. The absolute value of the (signed) curvature satisfies the familiar relation $|\kappa| = |\underline{\dot{t}}|/v$. From equation (2.1), we find for the time evolution of the argument φ of the tangent $\underline{t} = e^{i\varphi}$

$$\dot{\varphi} = v\,\kappa. \tag{2.2}$$

For constant curvature $\kappa(t) = \kappa_0 > 0$, the swimming path $\underline{r}(t)$ is a circle with radius $r_0 = 1/\kappa_0$. The angular frequency of circular swimming is $\omega_0 = v_0\kappa_0$ if speed $v(t) = v_0$ is constant. In the following, we consider the case where sperm cells swim in a counterclockwise sense along their circular swimming paths $\underline{r}(t)$ such that $\kappa_0 > 0$. Our results also apply for swimming in a clockwise sense, however, r_0 and ω_0 attain negative values in this case. Note that a change of sign $\kappa_0 \to -\kappa_0$ corresponds to using the complex-conjugate path $\underline{r} \to \underline{r}^*$.

We consider a sperm swimming path in a concentration field $c(\underline{x}) = c(x + iy)$ of chemoattractant. Due to the motion of the sperm cell, the local concentration $c(\underline{r}(t))$ at the position $\underline{r}(t)$ of the sperm cell changes with time t. Chemoattractant molecules bind to specific receptors on the flagellar membrane with a total rate $q(t)$ which is defined by an ensemble average and which we assume to be proportional to the local concentration

$$q(t) = \lambda\, c(\underline{r}(t)). \tag{2.3}$$

We introduce the chemoattractant stimulus $s(t) = \sum \delta(t - t_j)$ which counts binding events of single chemoattractant molecules to the receptors which occur at times t_j. Since binding events are stochastic, the stimulus $s(t)$ is a stochastic flux with expectation value

$$\langle s(t)\rangle = q(t). \tag{2.4}$$

This stimulus $s(t)$ triggers a response of the chemotactic signaling network. In general the signaling network is a dynamic system which generates a time-dependent output which depends on the history of the stimulus. We characterize this response by a dimensionless output variable $a(t)$ with $a = 1$ for a constant stimulus in the absence of fluctuations. This output variable $a(t)$ affects the curvature $\kappa(t)$ of the swimming path by modulating the activity of the flagellar motors. In our simple description [12], we write

$$\kappa(t) = \kappa_0 + \kappa_1(a(t) - 1) + \xi_m. \tag{2.5}$$

Here, we include a noise term ξ_m with zero mean in (2.5) to account for fluctuations of the flagellar beat due to fluctuations in the activity of the motor ensemble. For simplicity, we assume that the swimming speed $v(t) = v_0$ is constant, unaffected by chemotactic signaling.

We can capture the essential properties of the chemotactic signaling system, namely its ability to adapt and its relaxation dynamics, by a simple dynamical system [12]–[14]

$$\begin{aligned} \sigma\dot{a} &= p(s_b + s) - a + \xi_a, \\ \mu\dot{p} &= p(1 - a). \end{aligned} \tag{2.6}$$

Here, $p(t)$ is an internal variable which governs adaptation and represents a dynamic sensitivity. This sensitivity p is reduced whenever the output a of the signaling system exceeds the value 1, and correspondingly is increased if a falls below this value. In the absence of any stimulus, $s(t) = 0$, the sensitivity p remains bounded with $\langle p\rangle = 1/s_b$. The parameter s_b has units of a rate and corresponds to a detection limit for low stimuli which could for example result from a background activity of the chemoattractant receptors. The time constants σ and μ set the response timescale and the timescale of adaptation, respectively. The intrinsic fluctuations of

the molecular network underlying chemotactic signaling are included in a generic fashion by the noise term ξ_a with zero mean. For a time independent stimulus $s(t) = s_0$, the stochastic system (2.6) reaches a stationary state with $\langle a \rangle \approx 1$ and $\langle p \rangle \approx 1/(s_b + s_0)$. The system is adaptive since the expectation value (and also the full statistics) of the steady-state output is independent of the stimulus level s_0.

In the noise-free case, $\xi_a = 0$, $\xi_m = 0$, small periodic variations of the stimulus $s(t) = s_0 + s_1 \cos \omega_0 t$ evoke a periodic response of the curvature $\kappa(t) = \kappa_0 + \rho_\kappa s_1 \cos(\omega_0 t + \varphi_\kappa) + \mathcal{O}(s_1^2)$ with amplitude gain ρ_κ and phase shift φ_κ. The linear response coefficient $\tilde{\chi}_\kappa(\omega_0) = \rho_\kappa e^{i\varphi_\kappa}$ is obtained from the response function

$$\tilde{\chi}_\kappa(\omega) = \frac{\kappa_1}{s_b + s_0} \frac{i\omega\mu}{1 + i\omega\mu - \sigma\mu\omega^2} \tag{2.7}$$

of the signaling system described by equation (2.6), evaluated at the circling frequency ω_0. Note that the phase-shift φ_κ is independent of the stimulus strength s_0. The amplitude gain ρ_κ is a function of the stimulus level s_0 and can be written as

$$\rho_\kappa = \bar{\rho}_\kappa / (s_b + s_0) \tag{2.8}$$

with a constant $\bar{\rho}_\kappa$ that represents an amplification strength of the chemotactic signaling system.

2.2. Characterization of noise terms

2.2.1. Stochastic chemoattractant stimulus. Sperm cells 'measure' the local chemoattractant concentration $c = c(\underline{r}(t))$ by 'reading out' the number of their activated chemoattractant receptors. A chemoattractant receptor becomes activated upon binding a chemoattractant molecule and deactivates again on a timescale of 300 ms [7]. Activation and deactivation of receptors is subsumed together with downstream signaling in the generic signaling system (2.6) whose input $s(t)$ is the stochastic flux of binding events of individual chemoattractant molecules. Let us discuss first a homogeneous concentration field of chemoattractant $c(\underline{x}) = c_0$. We consider the case where the binding events of individual chemoattractant molecules to the receptors are independent and the series of binding events is therefore a Poissonian spike train $s(t) = \sum_j \delta(t - t_j)$ with expectation value equal to the rate $q_0 = \lambda c_0$ of binding events. Here, t_j denotes the time of the jth binding event.

In an inhomogeneous concentration field, the local chemoattractant concentration $c(\underline{r}(t))$ changes with time; thus $q(t)$ changes as well. We describe the statistics of the event times t_j by a non-homogeneous Poisson process, i.e. by a renewal process with conditional probability density

$$P(t_{j+1}|t_j) = q(t_{j+1}) \exp\left(- \int_{t_j}^{t_{j+1}} dt\, q(t) \right). \tag{2.9}$$

This choice gives $\langle s(t) \rangle = q(t)$ and a Poissonian statistics of binding times for slowly varying $q(t)$.

The generic signaling module (2.6) serves as a low-pass filter which averages the incoming stimulus over the relaxation time σ of the signaling module (2.6). Thus the relevant timescale to which the rate q of binding events should be compared is the relaxation time σ. When the rate q is large compared to σ^{-1} and $q(t)$ changes on a timescale slow compared to the mean

inter-event-interval $1/q$, then we can replace $s(t)$ by a coarse-grained version known as the diffusion limit

$$s(t) \approx q(t) + \sqrt{q(t)}\,\xi_s(t), \tag{2.10}$$

where $\xi_s(t)$ is Gaussian white noise with $\langle \xi_s(t_1)\xi_s(t_2)\rangle = \delta(t_1 - t_2)$. In this limit, the parameter $\eta = (q\sigma)^{-1/2}$ which characterizes the relative noise strength of $s(t)$ is small. Here, the relative noise strength of $s(t)$ averaged over a time τ is defined as

$$\langle \delta s\rangle_\tau^2 / \langle s\rangle_\tau^2 = (q\tau)^{-1} \tag{2.11}$$

with $\delta s = s - \langle s\rangle$, where $\langle\cdot\rangle_\tau$ denotes an average over a time interval τ. Hence, η^2 equals the relative noise strength of s for an averaging time $\tau = \sigma$.

2.2.2. Intrinsic noise of chemotactic signaling. Chemotactic signaling of sperm cells refers to the chain of events within the sperm's flagellum relating the activation of chemoattractant receptors to a motor response which changes the swimming path of the sperm cell. Early steps of the signaling cascade are likely to involve only low numbers of the messenger molecules cGMP [11]. Thus we expect, that the chemotactic signaling system is a source of fluctuations as well. We describe these fluctuations effectively by a noise term ξ_a with power spectrum $\tilde{S}_a(\omega)$. The power spectrum $\tilde{S}(\omega)$ of a process $\xi(t)$ is defined by $\langle \tilde{\xi}(\omega_1)\tilde{\xi}^*(\omega_2)\rangle = 2\pi\,\delta(\omega_1 - \omega_2)\,\tilde{S}(\omega_1)$ with $\tilde{\xi}(\omega) = \int_{-\infty}^{\infty} \mathrm{d}t\,\xi(t)\mathrm{e}^{-\mathrm{i}\omega t}$ being the Fourier transform of $\xi(t)$. Note $\int_{-\infty}^{\infty} \mathrm{d}\omega\,\tilde{S}(\omega) = 2\pi\,\langle \xi^2\rangle$.

2.2.3. Fluctuations of flagellar propulsion. Sperm cells are propelled in a liquid by the periodic beat of their flagellum, which is driven by an ensemble of dynein motors. We expect fluctuations in the propulsion generated by the flagellar beat due to noise in the activity of the motor ensemble. This noise causes fluctuations ξ_m, in the curvature of the swimming path $\underline{r}(t)$, which we characterize by the power spectrum $\tilde{S}_m(\omega)$ of ξ_m. In general, fluctuations in the activity of the motor ensemble will cause also fluctuations of the swimming speed $v(t)$. For simplicity, we neglect speed fluctuations here. Including speed fluctuations in our description is straightforward and does not change results significantly.

2.2.4. Hydrodynamic flows. In the open sea, complex hydrodynamic flows convect the sperm cell and perturb the concentration field of chemoattractant. Here, we do not take these effects into account.

Equations (2.1)–(2.6) describe stochastic sperm swimming paths in a concentration field of chemoattractant. The equations can be solved numerically; figure 1(B) shows an example of a stochastic swimming path $\underline{r}(t)$ in a linear concentration field of chemoattractant.

3. Statistical properties of sperm swimming paths

We first discuss in section 3.1 statistical properties of sperm swimming paths for circular swimming with fluctuating curvature. We relate the effective diffusion coefficient of sperm swimming circles to the fluctuation spectrum of the curvature. We then discuss diffusion and drift of swimming paths in a weak concentration gradient. We focus on two limit cases: (i) low chemoattractant concentration (section 3.2), and (ii) high chemoattractant concentration (section 3.3). We find analytical expressions for the effective diffusion coefficient for

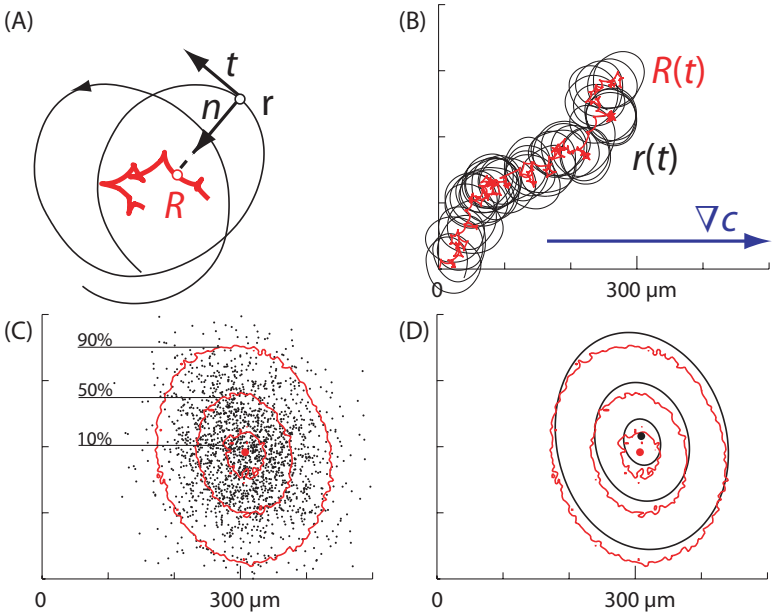

Figure 1. (A) Schematic depiction of a noisy circular swimming path $\underline{\mathrm{r}}(t)$ (black) and its moving center $\underline{\mathrm{R}}(t)$ (red). The centerline $\underline{\mathrm{R}}(t)$ is defined as $\underline{\mathrm{R}} = \underline{\mathrm{r}} + r_0 \mathrm{i}\underline{\mathrm{t}}$ in terms of the path $\underline{\mathrm{r}}(t)$ and its tangent $\underline{\mathrm{t}} = \dot{\underline{\mathrm{r}}}/v_0$, see equation (3.2). (B) Swimming path $\underline{\mathrm{r}}(t)$ (black) in a linear concentration field of chemoattractant. The direction of the concentration gradient is indicated by a blue arrow. The swimming path is a drifting circle. The drift of the circle can be described by the motion of its center $\underline{\mathrm{R}}(t)$ (red). The path shown is a numerical solution to equations (2.1)–(2.6) with parameters $\kappa_0 = 0.025\,\mu\mathrm{m}^{-1}$, $\kappa_1 = -2\kappa_0$, $v_0 = 100\,\mu\mathrm{m\,s}^{-1}$, $\sigma = \mu = 200\,\mathrm{ms}$, $s_\mathrm{b} = 10\,\mathrm{s}^{-1}$, $\lambda = 10\,\mathrm{pM}^{-1}\,\mathrm{s}^{-1}$, $\tilde{S}_a = 3 \times 10^{-3}\,\mathrm{s}$ and $\tilde{S}_\mathrm{m} = 0$. These parameter values are consistent with experimental findings, see the discussion. The linear concentration field is given by $c(x + \mathrm{i}y) = c_0 + c_1 x$ with $c_0 = 10\,\mathrm{pM}$, $c_1 = 0.1\,c_0/r_0$. Integration time was $t_\mathrm{end} = 100\,\mathrm{s}$. The initial conditions were $a(0) = 1$, $p(0) = 1/(s_\mathrm{b} + \lambda c_0)$, $\underline{\mathrm{r}}(0) = -r_0 \mathrm{i} e^{\mathrm{i}\varphi_0}$, and $\varphi_0 \in [0, 2\pi)$ drawn randomly from a uniform distribution. For the noise term ξ_a, Gaussian white noise with $\langle \xi_a(t_1)\xi_a(t_2)\rangle = \tilde{S}_a \delta(t_1 - t_2)$ was chosen. (C) Endpoints $\underline{\mathrm{R}}(t_\mathrm{end})$ of centerlines of swimming paths in a linear concentration field for $n = 10^4$ different realizations (black dots). All centerlines (not shown) start at the origin. The same parameters as for panel (B) were used. Also shown is the contour plot of a histogram of the centerline endpoints (red contour lines). The contour lines enclose regions which contain 10, 50 and 90% of the endpoints, respectively. The histogram was computed from $n = 10^6$ realizations. The expectation value $\langle \underline{\mathrm{R}}(t_\mathrm{end})\rangle$ is indicated by a red dot. (D) Contour plot of the spatial distribution function of the endpoints $\hat{\underline{\mathrm{R}}}(t_\mathrm{end})$ of the coarse-grained centerline $\hat{\underline{\mathrm{R}}}(t)$ determined by the effective equation of motion (4.1) (black contour lines). As in panel (C), the contour lines enclose regions, which contain 10, 50 and 90% of the endpoints, respectively. The distribution function of $\hat{\underline{\mathrm{R}}}(t_\mathrm{end})$ was obtained by numerically integrating the Fokker–Planck equation associated with (4.1). The expectation value $\langle \hat{\underline{\mathrm{R}}}(t_\mathrm{end})\rangle$ is indicated by a black dot. For comparison, the contour plot from panel (C) is shown again (red contour lines).

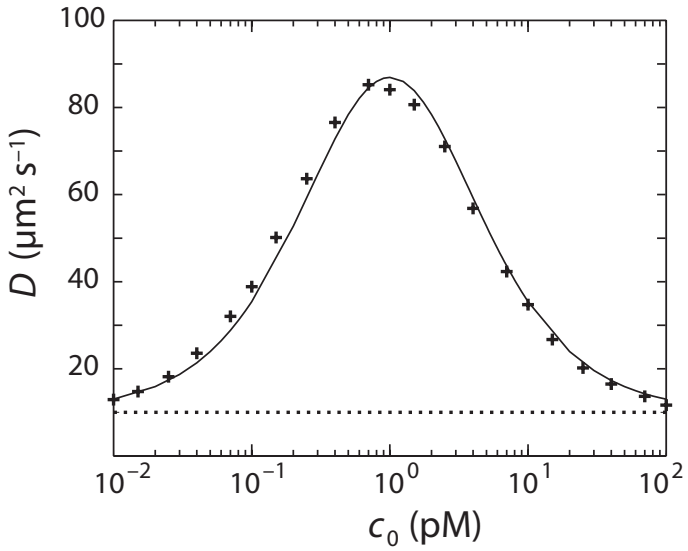

Figure 2. Diffusion constant D of sperm swimming circles as a function of concentration c_0 for a homogeneous concentration field of chemoattractant. Shown are simulation results (symbols) and our analytical result (solid line), see equations (3.9) and (3.25). Error bars are of the size of the symbols. The dotted line represents the analytic value for the diffusion constant in the absence of chemoattractant, $D^{(0)} = (r_0 v_0)^2 \tilde{S}_\kappa^{(0)}(\omega_0)/4$. The same parameter set as for figure 1 was used; these parameters are consistent with experimental findings.

cases (i) and (ii), which also describe very well numerical results for the diffusion coefficient at intermediate concentrations, see figure 2.

3.1. Circular swimming with fluctuating curvature

As an introductory example, we study planar sperm swimming paths $\underline{\mathrm{r}}(t)$ in the absence of a concentration gradient of chemoattractant: sperm cells then swim along circles of radius r_0 with a curvature $\kappa(t)$ that fluctuates around its mean $\kappa_0 = 1/r_0$

$$\kappa(t) = \kappa_0 + \xi_\kappa(t). \tag{3.1}$$

Here, ξ_κ is a stationary stochastic process with mean zero and power spectrum $\tilde{S}_\kappa(\omega)$ which represents the curvature fluctuations.

These curvature fluctuations result in an effective diffusion of the center $\underline{\mathrm{R}}(t)$ of the swimming circle. In the following, we characterize the diffusion of $\underline{\mathrm{R}}(t)$ in the limit of weak curvature fluctuations with the limit parameter ε small, where $\varepsilon^2 = r_0^2\langle\xi_\kappa^2\rangle$. We require the higher moments of ξ_κ to be of the order of at least ε^3, i.e. $r_0^n\langle\xi_\kappa^n\rangle \leqslant \mathcal{O}(\varepsilon^3)$, $n \geqslant 3$.

We introduce the moving center $\underline{\mathrm{R}}(t)$ of the swimming path $\underline{\mathrm{r}}(t)$, see figure 1(A)

$$\underline{\mathrm{R}} = \underline{\mathrm{r}} + r_0\underline{\mathrm{n}} = \underline{\mathrm{r}} + r_0\,\mathrm{i}\,\underline{\mathrm{t}}. \tag{3.2}$$

In the noise-free case, $\varepsilon = 0$, this definition yields the centerpoint $\underline{\mathrm{R}}$ of the perfect circle $\underline{\mathrm{r}}(t)$. By differentiation, we obtain the following stochastic differential equations for $\underline{\mathrm{R}}(t)$ and $\varphi(t)$

$$\begin{aligned} \dot{\varphi} &= v_0\kappa_0 + v_0\xi_\kappa, \\ \dot{\underline{\mathrm{R}}} &= -r_0 v_0\,\xi_\kappa\,\mathrm{e}^{\mathrm{i}\varphi}. \end{aligned} \tag{3.3}$$

Note that the second equation contains multiplicative noise. These equations also hold for the case where ξ_κ is Gaussian white noise provided the Stratonovich interpretation is used. We assume that the argument φ_0 of the tangent $\underline{t}(0) = e^{i\varphi_0}$ at time $t = 0$ is uniformly distributed in $[0, 2\pi)$. Without loss of generality, we choose $\underline{R}(0) = 0$. Then the rotational symmetry of the problem implies

$$\langle \underline{R} \rangle = 0. \tag{3.4}$$

The expectation value $\langle\cdot\rangle$ averages over an ensemble of stochastic paths with $\underline{R}(0) = 0$ and random φ_0 (uniformly distributed). In the following, we compute the variance matrix $C_{kl} = \langle R_k R_l \rangle$ where $k, l = 1, 2$ and $\underline{R} = R_1 + iR_2$. The trace of the variance matrix $C_{kk} = \langle |\underline{R}|^2 \rangle$ is computed as a double integral

$$\begin{aligned}\langle |\underline{R}(t)|^2 \rangle &= \int_0^t dt_1 \int_0^t dt_2 \, \langle \dot{\underline{R}}(t_1) \dot{\underline{R}}(t_2)^* \rangle \\ &= (r_0 v_0)^2 \int_0^t dt_1 \int_0^t dt_2 \, S_\kappa(t_2 - t_1) e^{i\omega_0(t_1 - t_2)} + \mathcal{O}(\varepsilon^3).\end{aligned} \tag{3.5}$$

Here, the autocorrelation function $S_\kappa(t_1 - t_2) = \langle \xi_\kappa(t_1) \xi_\kappa(t_2) \rangle$ is the Fourier transform of $\tilde{S}_\kappa(\omega)$. For times t much larger than the correlation time of ξ_κ, we can approximate $\langle |\underline{R}|^2 \rangle$ as

$$\langle |\underline{R}(t)|^2 \rangle \approx (r_0 v_0)^2 \int_0^t dt_1 \int_{-\infty}^{\infty} d\tau \, S_\kappa(\tau) e^{-i\omega_0 \tau} = (r_0 v_0)^2 \tilde{S}_\kappa(\omega_0) t. \tag{3.6}$$

Note that the variance $\langle |\underline{R}|^2 \rangle$ grows linearly in time as is typical for a diffusion process. The complex number $\langle \underline{R}^2 \rangle$ characterizes an anisotropy of the diffusion process

$$\langle \underline{R}^2 \rangle = \langle R_1^2 \rangle - \langle R_2^2 \rangle + 2i \langle R_1 R_2 \rangle. \tag{3.7}$$

To leading order in ε,

$$\langle \underline{R}(t)^2 \rangle \approx (r_0 v_0)^2 \int_0^t dt_1 \, \langle e^{2i\omega_0 t_1 + 2i\varphi_0} \rangle \, \tilde{S}_\kappa(\omega_0) = 0 \tag{3.8}$$

for a uniform distribution of φ_0. Indeed, the rotational symmetry of the problem already implies $\langle \underline{R}(t)^2 \rangle = 0$. We conclude, that curvature fluctuations result in effective isotropic diffusion of the center $\underline{R}(t)$ of the swimming circles with an effective diffusion constant D that is proportional to the power spectrum of the curvature fluctuations evaluated at the circle frequency $\omega_0 = v_0 \kappa_0$

$$4D \approx (v_0 r_0)^2 \tilde{S}_\kappa(\omega_0). \tag{3.9}$$

The approximation (3.9) is valid up to terms of order $\mathcal{O}(\varepsilon^3)$. Note that the diffusion coefficient is proportional to the power spectrum $\tilde{S}_\kappa$ of the curvature fluctuations evaluated at the frequency ω_0, see [15] for a related result in a different context. For the particular model given in (2.1)–(2.6), the power spectrum $\tilde{S}_\kappa(\omega)$ has contributions from (i) the stochastic stimulus, (ii) the intrinsic fluctuations of the chemotactic signaling system and (iii) from the fluctuations in the activity of the motor ensemble. Below we give an approximation for $\tilde{S}_\kappa$ in the limit of weak noise, see equation (3.25). In general, $\tilde{S}_\kappa$ and D are functions of the concentration c_0 of a homogeneous concentration field of chemoattractant. Figure 2 displays the concentration dependence of D; a pronounced maximum of D can be observed close to $c^* = s_b/\lambda$. Using the same reasoning as above, one can derive an exact expression for the diffusion constant D

$$4D = v_0^2 \tilde{C}_\kappa(\omega_0). \tag{3.10}$$

Here, $\tilde{C}_\kappa(\omega)$ is the Fourier transform of the characteristic function $C_\kappa(t) = \langle \exp \mathrm{i} v_0 \, \Phi_\kappa(t) \rangle$ of $\Phi_\kappa(t) = \int_0^t \mathrm{d}\tau \, \xi_\kappa(\tau)$. Expanding (3.10) in powers of ε reproduces (3.9) as leading order contribution. The special case where the curvature fluctuations ξ_κ are described by Gaussian white noise with $\langle \xi_\kappa(t_1) \, \xi_\kappa(t_2) \rangle = 2 D_\kappa \delta(t_1 - t_2)$, has been discussed in [16] and gives $C_\kappa(t) = \exp(-v_0^2 D_\kappa |t|)$ and $4D = 2 D_\kappa v_0^4 / (\omega_0^2 + D_\kappa^2 v_0^4)$.

3.2. Chemoattractant gradient with low concentration

There are strong indications, that sperm cells can detect single chemoattractant molecules, when chemoattractant concentration is subpicomolar [4, 7]. To characterize sperm chemotaxis at very low chemoattractant concentrations, we study the set of equations (2.1)–(2.6) in the limit of a low chemoattractant concentration with a chemoattractant molecule binding rate q small compared with σ^{-1}, where σ is the relaxation timescale of the signaling system in (2.6). For simplicity, we neglect the intrinsic noise of chemotactic signaling and the fluctuations in the activity of the motor ensemble, i.e. $\xi_a = 0$ and $\xi_\mathrm{m} = 0$.

3.2.1. The swimming response. For $q\sigma \ll 1$, every binding event evokes a stereotypic swimming response, which can be effectively described as a translation of the center $\underline{\mathrm{R}}$ of the swimming circle $\underline{\mathrm{r}}(t)$ by a vector $\Delta\underline{\mathrm{R}}$. The curvature response to a single stimulus spike $s(t) = \delta(t)$ is given by

$$\kappa(t) = \kappa_0 + \chi_\kappa(t). \tag{3.11}$$

Here, $\chi_\kappa(t) = (2\pi)^{-1} \int_{-\infty}^{\infty} \mathrm{d}\omega \tilde{\chi}_\kappa(\omega) \, \mathrm{e}^{\mathrm{i}\omega t}$ is the time-domain linear response function of the chemotactic signaling system (2.6). The tangent $\underline{\mathrm{t}} = \dot{\underline{\mathrm{r}}}/v_0$ integrates as

$$\underline{\mathrm{t}}(t) = \exp(\mathrm{i}\omega_0 t + \mathrm{i}\varphi_0) \exp\left(\mathrm{i} v_0 \int_{-\infty}^{t} \mathrm{d}t_0 \, \chi_\kappa(t_0) \right). \tag{3.12}$$

We may assume $\underline{\mathrm{R}}(t) = 0$ before the stimulus spike occurred; hence $\underline{\mathrm{r}}(t) = -\mathrm{i} r_0 \exp(\mathrm{i}\omega_0 + \mathrm{i}\varphi_0)$ for $t < 0$. For times long after the stimulus spike, $t \gg \sigma$, the swimming path resumes a perfect circular trajectory again

$$\underline{\mathrm{r}}(t) = \underline{\mathrm{u}} \, \mathrm{e}^{\mathrm{i}\varphi_0} - \mathrm{i} r_0 \, \exp(\mathrm{i}\omega_0 t + \mathrm{i}\varphi_0 + \mathrm{i}\varphi_u) \tag{3.13}$$

with a phase shift $\varphi_u = v_0 \tilde{\chi}_\kappa(0)$ and a translation vector $\Delta\underline{\mathrm{R}} = \underline{\mathrm{u}} \, \mathrm{e}^{\mathrm{i}\varphi_0}$. By integrating equation (3.12), we find $\underline{\mathrm{u}} \approx -r_0 v_0 \tilde{\chi}_\kappa^*(\omega_0)$ to leading order in $v_0 |\chi_\kappa|$. Here $\tilde{\chi}_\kappa(\omega_0) = \rho_\kappa \mathrm{e}^{\mathrm{i}\varphi_\kappa}$ is the linear response coefficient at the circling frequency ω_0 of the generic signaling module given in (2.6), see (2.7). For an adapting signaling system such as (2.6), we have $\varphi_u = 0$.

3.2.2. Statistics of sperm swimming paths. We study the stochastic equations of motion (2.1)–(2.6) of sperm swimming paths for a linear concentration field of chemoattractant,

$$c(\underline{\mathrm{x}}) = c(x + \mathrm{i}y) = c_0 + c_1 x, \tag{3.14}$$

where we assume for simplicity that the gradient is parallel to the x-axis. We consider the limit of (i) a shallow concentration gradient with $\nu = c_1 r_0 / c_0 \ll 1$, and (ii) a binding rate $q(t)$ of chemoattractant molecules low compared with σ^{-1}. Between two binding events, $t_j \ll t < t_{j+1}$, the swimming path is circular once the jth swimming response relaxes

$$\underline{\mathrm{r}}(t) = \underline{\mathrm{R}}(t) - \mathrm{i} r_0 \, \mathrm{e}^{\mathrm{i}\omega_0 t + \mathrm{i}\varphi_0}. \tag{3.15}$$

This results in a periodic modulation of the binding rate

$$q(t) = \lambda\, c(\underline{\mathrm{r}}(t)) = \lambda\, c(\underline{\mathrm{R}}(t)) + \lambda\, c_1 r_0\, \sin(\omega_0 t + \varphi_0). \tag{3.16}$$

For $q\,\sigma \ll 1$, we can treat individual binding events independently and find for the center $\underline{\mathrm{R}}$ of the circular swimming path $\underline{\mathrm{r}}$ for $t > 0$

$$\underline{\mathrm{R}}(t) = \underline{\mathrm{u}} \sum_{0<t_j<t} \mathrm{e}^{\mathrm{i}\varphi_j}. \tag{3.17}$$

Here, the t_j denotes the times of the individual binding events and $\varphi_j = \varphi(t_j)$. From the periodic modulation of the binding rate (3.16), we determine the probability density $P(\varphi)$ of the angles φ_j

$$2\pi\; P(\varphi) = 1 + \nu \sin\varphi + \mathcal{O}(\nu^2). \tag{3.18}$$

The number n of binding events in the time interval $0 < t_j < t$ satisfies $\langle n\rangle = \langle \delta n^2\rangle = \lambda c_0\, t + \mathcal{O}(\nu)$, where $\delta n = n - \langle n\rangle$. Thus we find using (3.17) and (3.18)

$$\begin{aligned} \langle \underline{\mathrm{R}}(t)\rangle &= \underline{\mathrm{u}}\lambda c_0 t \int_0^{2\pi} \mathrm{d}\varphi\, P(\varphi)\mathrm{e}^{\mathrm{i}\varphi} + \mathcal{O}(\nu^2) \\ &= \underline{\mathrm{u}}\lambda c_0 t\, \mathrm{i}\nu/2 + \mathcal{O}(\nu^2), \quad \text{and} \\ \langle |\delta\underline{\mathrm{R}}(t)|^2\rangle &= |\underline{\mathrm{u}}|^2 \lambda c_0 t + \mathcal{O}(\nu^2). \end{aligned} \tag{3.19}$$

with $\delta\underline{\mathrm{R}} = \underline{\mathrm{R}} - \langle \underline{\mathrm{R}}\rangle$. Thus, the circle center $\underline{\mathrm{R}}$ is both (i) drifting with drift speed $v_\mathrm{d} = \rho_\kappa \lambda c_1 r_0^2 v_0/2$ in a direction which encloses an angle $\alpha = 3\pi/2 - \varphi_\kappa$ with the concentration gradient and (ii) diffusing in both space dimensions with an effective diffusion coefficient $D = \langle |\delta\underline{\mathrm{R}}|^2\rangle/(4t) = (r_0 v_0)^2 \rho_\kappa^2 \lambda c_0/4 + \mathcal{O}(\nu^2)$. The average drift of the circle center given by (3.19) is the same as the one obtained for a deterministic description of sperm chemotaxis [12]. Thus the deterministic approach is providing a mean-field description. Diffusion is essentially isotropic; the quantity $\langle \delta\underline{\mathrm{R}}^2\rangle = \langle \delta R_1^2\rangle - \langle \delta R_2^2\rangle + 2\mathrm{i}\langle \delta R_1\, \delta R_2\rangle$, which characterizes anisotropy of diffusion vanishes to linear order in ν, $\langle \delta\underline{\mathrm{R}}^2\rangle = 0 + \mathcal{O}(\nu^2)$. The relative strength of the chemotactic drift compared to the undirected diffusive motion of the center of the swimming circle is characterized by a dimensionless Peclet number

$$\mathrm{Pe} = \frac{v_\mathrm{d} r_0}{4D} = \frac{s_\mathrm{b} + \lambda c}{2\bar{\rho}_\kappa \omega_0} \frac{|\nabla c|}{c} + \mathcal{O}(\nu^2). \tag{3.20}$$

This expression for the Peclet number only holds if intrinsic fluctuations of chemotactic signaling and noise in the activity of the flagellar motor ensemble can be neglected. In the next section, we derive an expression for the effective diffusion coefficient D where these noise sources have been included, see equations (3.25) and (3.26). With these noise sources, we find that the Peclet number is proportional to the relative concentration gradient $|\nabla c|/c$ for high concentrations c.

3.3. Chemoattractant gradient with high concentration

To gain further insight into the stochastic description of sperm chemotaxis, we study the set of equations (2.1)–(2.6) in the weak noise limit for a linear concentration field of chemoattractant $c(x + \mathrm{i}y) = c_0 + c_1 x$. More precisely, we consider the limit of (i) a shallow concentration gradient with $\nu = c_1 r_0/c_0 \ll 1$, and (ii) a high chemoattractant concentration c_0 with a binding rate $q(t) = \lambda c(\underline{\mathrm{r}}(t))$ of chemoattractant molecules much higher than σ^{-1}, where σ sets the

relaxation timescale of the chemotactic signaling system in (2.6). In this limit, the parameter $\eta = (q\sigma)^{-1/2}$ is small; η characterizes the relative noise strength of $s(t)$. For simplicity, we first neglect the intrinsic noise of chemotactic signaling and the fluctuations in the activity of the motor ensemble, i.e. $\xi_a = 0$ and $\xi_\mathrm{m} = 0$. The general case will be studied in equation (3.25). We develop a systematic perturbation theory for the statistics of centerlines $\underline{\mathrm{R}}(t)$ of stochastic swimming paths for the small limit parameters ν and η. In a systematic expansion of $\langle\underline{\mathrm{R}}\rangle$, $\langle|\delta\underline{\mathrm{R}}|^2\rangle$ and $\langle\delta\underline{\mathrm{R}}^2\rangle$ in powers of ν and η, many terms vanish due to the symmetries of the problem; to leading order we find

$$\begin{aligned}
&\langle\underline{\mathrm{R}}(t)\rangle \sim \nu\, t + \mathcal{O}(\nu\eta^2, \nu^3),\\
&\langle|\delta\underline{\mathrm{R}}(t)|^2\rangle \sim \eta^2\, t + \mathcal{O}(\nu^2\eta^2, \eta^3),\\
&\langle\delta\underline{\mathrm{R}}(t)^2\rangle = 0 + \mathcal{O}(\nu^2\eta^2).
\end{aligned} \tag{3.21}$$

The expansion of $\langle\underline{\mathrm{R}}\rangle$ in powers of ν can only contain odd powers of ν since reversing the direction of the gradient changes the sign of both ν and $\langle\underline{\mathrm{R}}\rangle$. Likewise the expansions of both $\langle|\underline{\mathrm{R}}|^2\rangle$ and $\langle\underline{\mathrm{R}}^2\rangle$ contain only even powers of ν. Terms proportional to η yield zero in the noise-average. Since $\langle\delta\underline{\mathrm{R}}^2\rangle$ measures anisotropy, this expression must vanish in the case $\nu = 0$ when the rotational symmetry is not broken. For the leading order coefficients of $\langle\underline{\mathrm{R}}\rangle$ and $\langle|\underline{\mathrm{R}}|^2\rangle$ we recover essentially the results obtained for the case of low concentration

$$\langle\underline{\mathrm{R}}(t)\rangle = -\mathrm{i}\, v_\mathrm{d}\, \mathrm{e}^{-\mathrm{i}\varphi_\kappa}\, t + \mathcal{O}(\nu\eta^2, \nu^3), \tag{3.22}$$

$$\langle|\delta\underline{\mathrm{R}}(t)|^2\rangle = (r_0 v_0)^2\, \tilde{S}_\kappa(\omega_0)\, t + \mathcal{O}(\nu^2\eta^2, \eta^3) \tag{3.23}$$

with chemotactic drift speed

$$v_\mathrm{d} = \rho_\kappa \lambda c_1 r_0^2 v_0/2 \tag{3.24}$$

and $\tilde{S}_\kappa(\omega_0) = \rho_\kappa^2 \lambda c_0$. The derivation of (3.22), (3.23) is similar to the calculations in sections 3.1 and 3.2.

So far, we have neglected the intrinsic noise of chemotactic signaling and the fluctuations in the activity of the motor ensemble. Now we include these noise terms and consider the limit of weak noise with $\eta \ll 1$, $\langle\xi_a^2\rangle \lesssim \eta^2$ and $r_0^2\langle\xi_\mathrm{m}^2\rangle \lesssim \eta^2$. We also assume that the higher order moments of ξ_a and ξ_m are of the order of at least $\mathcal{O}(\eta^3)$. In this limit, $\tilde{S}_\kappa(\omega)$ is a sum of contributions from the different noise sources

$$\tilde{S}_\kappa(\omega_0) = \rho_\kappa^2 \lambda c_0 + \bar{\rho}_\kappa^2 \tilde{S}_a(\omega_0) + \tilde{S}_\mathrm{m}(\omega_0) + \mathcal{O}(\nu^2, \eta^3), \tag{3.25}$$

where $\rho_\kappa = \bar{\rho}_\kappa/(s_\mathrm{b} + \lambda c_0)$ is the amplitude gain of the chemotactic signaling system (2.6). The second summand of the right-hand side of equation (3.25) describes a contribution to $\tilde{S}_\kappa$ stemming from the intrinsic noise of chemotactic signaling; whereas the third summand describes a contribution due to fluctuations in the activity of the motor ensemble. We define the concentration independent part of $\tilde{S}_\kappa(\omega_0)$ as $\tilde{S}_\kappa(\omega_0)^{(0)} = \bar{\rho}_\kappa^2 \tilde{S}_a(\omega_0) + \tilde{S}_\mathrm{m}(\omega_0)$. We can thus write $\tilde{S}_\kappa(\omega_0)$ as the sum of a concentration independent part $\tilde{S}_\kappa(\omega_0)^{(0)}$ and a concentration-dependent part $\tilde{S}_\kappa(\omega_0)^{(c)} = \rho_\kappa^2 \lambda c_0$. From $\rho_\kappa = \bar{\rho}_\kappa/(s_\mathrm{b} + \lambda c_0)$, we see that $\tilde{S}_\kappa(\omega_0)^{(c)}$ scales like $c_0/(s_\mathrm{b} + \lambda c_0)^2$. As a consequence, $\tilde{S}_\kappa(\omega_0)$ is a non-monotonic function of concentration c_0 with a maximum at $c^* = s_\mathrm{b}/\lambda$. Hence, also the effective diffusion constant

$$D = \langle|\delta\underline{\mathrm{R}}|^2\rangle/(4t) = (r_0 v_0)^2 \tilde{S}_\kappa(\omega_0)/4 + \mathcal{O}(\nu^2\eta^2, \eta^3) \tag{3.26}$$

depends on concentration c_0 via $\tilde{S}_\kappa(\omega_0)$, see figure 2. Note that in the absence of a concentration gradient, equation (3.26) corresponds to the earlier result (3.9) from section 3.1. Our estimate

for the fluctuation spectrum of the curvature given in equation (3.25) also describes the regime of low chemoattractant concentration[2]. Interestingly, our numerical simulations show that equation (3.25) also provides a good approximation in the regime of intermediate concentrations, see figure 2.

4. Effective equation for the centerline

We derive an effective equation of motion for a coarse-grained centerline $\underline{\hat{\mathrm{R}}}(t)$ in a linear concentration field (3.14). We restrict ourselves to the limit case of weak noise with $\eta \ll 1$ as specified in the previous section 3.3. Additionally, we assume that the concentration gradient is shallow with $\nu = c_1 r_0/c_0 \ll 1$. On short timescales $t < T = 2\pi/\omega_0$, the centerline $\underline{\mathrm{R}}(t)$ is a stochastic trajectory that depends on the particular shape of the spectra $\tilde{S}_a$ and $\tilde{S}_{\mathrm{m}}$ and therefore has non-generic properties. For longer time intervals $\Delta t = nT$, however, we find simple, general expressions for the drift $\langle \underline{\mathrm{R}}(\Delta t) - \underline{\mathrm{R}}(0)\rangle$ and for the variance $\langle |\underline{\mathrm{R}}(\Delta t)|^2\rangle$, see equations (3.22)–(3.23).

In order to derive a genuine coarse-grained description, we introduce a discrete centerline $\underline{\hat{\mathrm{R}}}(t_k)$, which is defined at the discrete times $t_k = k\,\Delta t$, $k = 0, 1, 2, \ldots$, and which reproduces (to leading order) the second-order statistics of $\underline{\mathrm{R}}(t)$ at the discrete times t_k, see appendix A for details. We then perform a continuum limit to find a continuous-time coarse-grained centerline $\underline{\hat{\mathrm{R}}}(t)$ which obeys

$$\frac{\mathrm{d}}{\mathrm{d}t}\,\underline{\hat{\mathrm{R}}}(t) = v_{\mathrm{d}}\,\mathrm{e}^{\mathrm{i}\alpha}\,\underline{\nabla} c/|\underline{\nabla} c| + \underline{\xi}. \tag{4.1}$$

Here $\underline{\xi} = \xi_1 + \mathrm{i}\,\xi_2$ is a complex random variable whose components ξ_j are uncorrelated Gaussian random variables with $\langle \xi_k(t_1)\xi_l(t_2)\rangle = 2D\,\delta(t_1 - t_2)\,\delta_{kl}$ for $k, l = 1, 2$. The concentration gradient $\underline{\nabla} c$ is the complex number $\underline{\nabla} c(x + \mathrm{i}y) = \partial_x c(x + \mathrm{i}y) + \mathrm{i}\,\partial_y c(x + \mathrm{i}y)$. The time-evolution of the coarse-grained centerline $\underline{\hat{\mathrm{R}}}$ described by equation (4.1) is the superposition of (i) a deterministic drift with drift velocity v_{d} in a direction that encloses an angle of $\alpha = \frac{3}{2}\pi - \varphi_\kappa$ with the concentration gradient, and (ii) pure diffusion with an effective diffusion coefficient of D. Since the diffusion coefficient D depends on concentration, the noise term in equation (4.1) is effectively multiplicative. Equation (4.1) is defined by using the Itō interpretation; see [17, 18] for a discussion of Itō and Stratonovich stochastic differential equations. Note that the Itō and the Stratonovich version of (4.1) differ by a noise-induced drift term which is of the order of $\sim \nu\eta^2$. We can generalize (4.1) for a nonlinear concentration field $c(\underline{\mathrm{x}})$, provided the nonlinearities of the concentration field are small on the length scale r_0, i.e. $|\nabla^2 c| \ll |\nabla c|/r_0$.

Figure 1(D) compares (i) the distribution of endpoints $\underline{\mathrm{R}}(t_{\mathrm{end}})$ of centerlines $\underline{\mathrm{R}}(t)$ of stochastic swimming paths $\underline{\mathrm{r}}(t)$ obtained from the full dynamic equations of stochastic sperm motion (2.1)–(2.6), and (ii) the distribution of endpoints $\underline{\hat{\mathrm{R}}}(t_{\mathrm{end}})$ of coarse-grained centerlines $\underline{\hat{\mathrm{R}}}(t)$ obtained from the effective equation of motion (4.1). We find good agreement between both endpoint distributions. In particular, both endpoint distributions are anisotropic. This is remarkable, since the distribution of endpoints $\underline{\hat{\mathrm{R}}}(t_{\mathrm{end}})$ of coarse-grained centerlines is obtained from simulating equation (4.1), which has an isotropic noise term. The apparent anisotropy is a consequence of the position dependence of the drift speed $v_{\mathrm{d}}(\underline{\mathrm{R}})$. Note that in the special case

[2] Equations (3.22), (3.23) and (3.25) also hold in the case of weak output noise with $\langle \delta a^2\rangle \ll 1$, where $\delta a = a - \langle a\rangle$. In this limit, the noise strength is given by $\eta^2 = q/[(s_{\mathrm{b}} + q)^2\sigma]$. Note that $\langle \delta a^2\rangle \approx \eta^2/2$, if only fluctuations of the chemotactic stimulus are considered.

$\alpha = 0$, the stochastic equation of motion (4.1) of the coarse-grained centerline $\hat{\underline{\mathrm{R}}}$ describes the trajectory of a particle diffusing in an effective potential $E = \Theta \nabla \ln(s_\mathrm{b} + \lambda c)$ which satisfies $-\nabla E(\underline{\mathrm{R}}) = v_\mathrm{d} \nabla c/|\nabla c|$. Here $\Theta = \bar{\rho}_\kappa r_0^2 v_0/2$ is a constant.

5. Example: radial concentration field

We discuss the case of a radial concentration field $c(\underline{\mathrm{x}}) = C(|\underline{\mathrm{x}}|)$, which arises if chemoattractant diffuses away from a single source such as an egg. The chemotactic drift speed v_d and the effective diffusion coefficient D of sperm swimming circles depend on the concentration c, see equations (3.24) and (3.26). In a radial concentration field, these quantities become functions $v_\mathrm{d} = v_\mathrm{d}(R)$ and $D = D(R)$ of the distance $R = |\underline{\mathrm{R}}|$ from the source. We introduce polar coordinates (R, ψ) such that $\underline{\mathrm{R}} = R\,\mathrm{e}^{\mathrm{i}\psi}$. From (4.1) and the rules of stochastic calculus [17], we find a stochastic differential equation for R and ψ in the Itō interpretation, see appendix B

$$\begin{aligned} \dot{R} &= v_\mathrm{d} \sin\varphi_\kappa + \xi_1 + D/R, \\ \dot{\psi} &= (v_\mathrm{d} \cos\varphi_\kappa + \xi_2)/R, \end{aligned} \tag{5.1}$$

where ξ_1 and ξ_2 are uncorrelated Gaussian white noise terms with zero mean and $\langle \xi_k(t_1)\, \xi_l(t_2)\rangle = 2D\,\delta(t_1 - t_2)\,\delta_{kl}$. The expression for $\dot{R}$ in equation (5.1) contains a noise-induced drift term D/R, which results from the nonlinearity of the coordinate transformation $\underline{\mathrm{R}} = R\,\mathrm{e}^{\mathrm{i}\psi} \mapsto (R, \psi)$. We introduce the probability density $S(\underline{\mathrm{R}}, t)$ such that $S\,\mathrm{d}A$ is the probability to find a sperm cell in the area element $\mathrm{d}A$ at time t. The total number of sperm cells in the system equals $\int \mathrm{d}A\, S(\underline{\mathrm{R}}, t)$. It is useful to introduce also the radial probability density $P(R, t) = R \int_0^{2\pi} \mathrm{d}\psi\, S(R\mathrm{e}^{\mathrm{i}\psi}, t)$. Note that $P\,\mathrm{d}R$ is the probability to find a sperm cell in a thin annulus of radius R and width $\mathrm{d}R$. In our effective equation of motion (5.1), the dynamics of R decouples from ψ reflecting the symmetries of the problem. Therefore, the radial probability $P(R, t)$ obeys a Fokker–Planck equation which reads [19]

$$\frac{\partial}{\partial t} P = \mathcal{L}\, P \tag{5.2}$$

with a Fokker–Planck operator $\mathcal{L}$ given by

$$\mathcal{L} = \frac{\partial}{\partial R}\left[-\left(v_\mathrm{d}(R) \sin\varphi_\kappa + D(R)/R\right) + \frac{\partial}{\partial R} D(R) \right]. \tag{5.3}$$

For completeness, we mention that the equation for the probability density $S(\underline{\mathrm{R}}, t) = S(R\mathrm{e}^{\mathrm{i}\psi}, t)$ has the form $R\frac{\partial}{\partial t} S = \mathcal{L}(RS) + \frac{\partial}{\partial \psi}\left(-v_\mathrm{d} \cos\varphi_\kappa RS + \frac{\partial}{\partial \psi} DS\right)$.

We are interested in the rate at which sperm cells reach the egg and study in the following an idealized scenario, where (i) we neglect the concentration dependence of the effective diffusion coefficient $D(R) = D_0$, (ii) the sensitivity threshold of chemotactic signaling vanishes, $s_\mathrm{b} = 0$, and (iii) the radial chemoattractant concentration field decays as a power-law $c(\underline{\mathrm{x}}) \sim 1/|\underline{\mathrm{x}}|^\beta$ with exponent β. Note that the steady-state concentration field established by diffusion in three-dimensional space from a spherical chemoattractant source with constant release rate of chemoattractant corresponds to $\beta = 1$. For adaptive chemotactic signaling (without sensitivity threshold), the relevant input quantity is the relative concentration gradient $|\nabla c|/c$, which for our choice of concentration field scales inversely with distance as $|\nabla c|/c = \beta/R$. Hence, the drift speed in the radial direction reads $v_\mathrm{d} \sin\varphi_\kappa = -\Gamma_0/R$ where $\Gamma_0 = -\beta \bar{\rho}_\kappa r_0^2\, v_0 \sin\varphi_\kappa$

is a constant. Likewise, the drift speed in the azimuthal direction is given by $v_d \cos\varphi_\kappa = -\Gamma_0 \cot\varphi_\kappa / R$.

To mimic the egg, we consider a disk-shaped target of radius R_{target} located at the origin of the concentration field which absorbs any sperm cell hitting its boundary. The absorbing target gives rise to a boundary condition $P(R_{\text{target}}) = 0$. We study the steady-state solution of equation (5.2) subject to this boundary condition and the condition $P_0(R) \approx 2\pi R\, S_\infty$ for large R where S_∞ is the sperm concentration far from the target. For positive chemotaxis with $\Gamma_0 > 0$, the stationary probability density reads $S_0(\underline{\mathrm{R}}) = P_0(R)/(2\pi R)$

$$S_0(\underline{\mathrm{R}}) = S_\infty \left[1 - \left(\frac{R_{\text{target}}}{|\underline{\mathrm{R}}|} \right)^{\Gamma_0/D_0} \right]. \tag{5.4}$$

In steady-state, sperm cells arrive at the target with a constant rate $k_0 = 2\pi\, S_\infty\, \Gamma_0$. The stationary state is characterized by a net flux in the azimuthal direction $J_\psi = v_d \cos\varphi_\kappa\, S_0(\underline{\mathrm{R}})$, i.e. $k_\psi = J_\psi\, \mathrm{d}R$ is the rate by which sperm cells pass through a section of length $\mathrm{d}R$ on a ray emanating from the origin. Thus there is a net circular current whirling around the origin. Such an azimuthal flux has been already discussed previously [20]. Note that if chemotaxis is absent or negative with $\Gamma_0 \leqslant 0$, then there exists no steady-state probability distribution $S_0(\underline{\mathrm{R}})$ for fixed concentration S_∞ at infinity. If we start in this case with a homogenous distribution of sperm cells $S(\underline{\mathrm{R}}, 0) = S_\infty$ at time $t = 0$, a growing region around the target becomes depleted of sperm cells and the time-dependent rate $k(t)$ of sperm cells arriving at the target vanishes in the limit of long times. We thus find that the system undergoes a dynamic second-order phase transition as a function of chemotactic strength Γ_0 where $k_0 = \lim_{t\to\infty} k(t)$ plays the role of an order parameter.

6. Discussion

In most experimental studies of sperm swimming in a chemoattractant field, sperm cells become localized near a boundary surface and swim in a plane [1], [4]–[11]. Observed swimming paths exhibit a large variability. Here, we presented a description of sperm chemotaxis in a plane which takes into account sources of fluctuations such as (i) a finite precision of the cell's measurement of the local chemoattractant concentration, (ii) intrinsic noise of chemotactic signaling, and (iii) fluctuations in the activity of the propulsion mechanism. In the absence of such fluctuations, sperm swimming paths are trochoids, or drifting circles [12]. In the presence of fluctuations, the paths can be described as noisy trochoids, resulting from the superposition of a chemotactic drift and unbiased random motion. We find expressions for the chemotactic drift velocity and the effective diffusion coefficient in the limit of a weak concentration gradient. Note that the assumption of a weak concentration gradient is satisfied in most experimental conditions, except perhaps in the close vicinity of a chemoattractant source such as an egg or a micropipette releasing chemoattractant.

We can estimate parameters relevant for our stochastic description of sperm chemotaxis. In experiments on sea urchin sperm, typical values observed for the swimming speed and radius of swimming circles are $v_0 \approx 100$–$200\,\mu\mathrm{m\,s^{-1}}$, $r_0 \approx 20$–$40\,\mu\mathrm{m}$, respectively [1, 21]. For comparison, the radius of the egg is $R_{\text{egg}} \approx 100\,\mu\mathrm{m}$ [22]. From the drift speed $v_d \approx 25$–$50\,\mu\mathrm{m\,s^{-1}}$ of swimming circles in a concentration gradient with $|\nabla c|/c \sim 1/100\,\mu\mathrm{m}$ reported in [1], we can estimate the amplification strength of the chemotactic signaling system as $\bar{\rho}_\kappa \approx 2v_d/(r_0^2 v_0 |\nabla c|/c) \approx 0.05\,\mu\mathrm{m}^{-1}$. The drift angle α was found to peak around $\alpha \approx 0$ [1, 10].

From stopped-flow experiments, it is known that chemotactic signaling operates on timescales 0.1–0.5 s [5], we thus expect the intrinsic relaxation times of the chemotactic signaling system (2.6) σ, μ to fall in that range. Sperm cells probably respond to single chemoattractant molecules [4, 7], we therefore expect $s_b \lesssim 1/\sigma$. Chemoattractant molecules bind to receptors on the sperm flagellum at a rate $q(t)$, proportional to concentration $q(t) = \lambda c(\underline{r}(t))$. where $\lambda \approx 20\,\mathrm{pM}^{-1}\,\mathrm{s}$ has been estimated [1]. In an experiment with sea urchin sperm in a shallow observation chamber in the absence of chemoattractant, sperm cells were observed to swim along circular paths $\underline{r}(t)$ with radius $r_0 = 40\,\mu\mathrm{m}$ and a swimming speed $v_0 = 100\,\mu\mathrm{m\,s}^{-1}$. For long time, the center $\underline{R}(t)$ of the swimming circle diffused with an effective diffusion constant $D = 9 \pm 2\,\mu\mathrm{m}^2\,\mathrm{s}^{-1}$ [23]. Using equation (3.26), we find that the swimming noise stemming from the intrinsic fluctuations of chemotactic signaling and the fluctuations in the activity of the flagellar motor ensemble is characterized by $\tilde{S}_\kappa^{(0)}(\omega_0) = \bar{\rho}_\kappa^2 \tilde{S}_a(\omega_0) + \tilde{S}_\mathrm{m}(\omega_0) \approx 2.5 \times 10^{-6}\,\mathrm{s}\,\mu\mathrm{m}^{-2}$.

In a homogeneous concentration field of chemoattractant, our theory predicts a diffusion coefficient of the center of the swimming circle which depends on concentration in a non-monotonic way with a maximum at a finite concentration $c^* = s_b/\lambda$, see figure 2. This concentration dependence of the diffusion constant results from the fact that fluctuations of the chemotactic stimulus elicit a stochastic chemotactic response and contribute to the effective diffusion constant. For low concentrations $c_0 \ll c^*$, the chemotactic stimulus and its fluctuations are small, producing only a negligible contribution to the effective diffusion constant. For high concentrations $c_0 \gg c^*$, the chemotactic signaling system adapts its sensitivity to an averaged stimulus and thus generates an output with small fluctuations. The concentration dependence of the effective diffusion constant of sperm swimming paths could be tested in future experiments. With the parameter estimates given above, we find a value for c^* in the subpicomolar range, $c^* = 0.1$–$1\,\mathrm{pM}$.

The motion of sperm cells in a concentration gradient is characterized by a Peclet number which compares drift speed and the effective diffusion coefficient on the scale sperm swimming circles. For fixed relative strength $|\nabla c|/c$ of the concentration gradient, this Peclet number increases with concentration c and saturates for high concentrations $c \gg c^*$. For a concentration gradient with $|\nabla c|/c = 1/100\,\mu\mathrm{m}$ as employed in [1], we estimate $\mathrm{Pe} \approx 1$ at $c \approx c^*$ and $\mathrm{Pe} \approx 10$–100 for $c \gg c^*$.

In the absence of fluctuations, chemotaxis of sea urchin sperm cells relies on a robust mechanism which depends only on a few generic properties of the signaling system and does not require fine-tuning of parameters [12]: the swimming circles of sperm cells drift toward regions of higher chemoattractant concentration whenever $-\pi < \varphi_\kappa < 0$, where φ_κ is the phaseshift between a periodic stimulus and the output generated by the chemotactic signaling system. The equation (2.6) used in this work to describe the signaling system differs slightly from the one employed in [12]. In particular, the timescale of adaptation is independent of the stimulus level for the signaling system used here. It has been shown in stopped-flow experiments that the timescales of the chemotactic response change only marginally when stimulus strength is varied from picomolar to micromolar concentrations [1]. Additionally, the phase-shift φ_κ does not depend on the stimulus level for the modified signaling system (2.6). We expect that for the chemotactic signaling system of sea urchin sperm this phase-shift is largely independent of chemoattractant concentration to ensure successful chemotaxis at different concentrations.

The chemotactic strategy of sea urchin sperm cells differs fundamentally from the mechanism employed by bacteria such as *Escherichia coli* [24, 25]. These bacteria perform

a biased random walk switching stochastically between a running mode with net motion and a tumbling mode during which the cell is randomly reoriented. Chemotaxis in a concentration gradient of chemoattractant is achieved by adjusting the rate of tumbling events in a way that depends on the history of the chemotactic stimulus. Thus bacterial chemotaxis is intrinsically stochastic and cannot be understood without considering noise. The mechanism of sperm chemotaxis, on the other hand, does not require noise. As we show here, this mechanism nevertheless also shows a high degree of robustness in the presence of fluctuations.

So far, we have discussed planar swimming paths of sperm cells close to a surface. Far from boundary surfaces, sea urchin sperm cells swim along helical paths [26, 27] as a consequence of the chirality of their flagellar beat [7, 28, 29]. When swimming in a concentration gradient of chemoattractant, the helical swimming path tends to align with the gradient direction [26, 30]. Theory predicts that the rate of alignment depends on the strength of the concentration gradient. The speed of net displacement along the helix centerline, however, is almost unaffected by the concentration gradient [12]. Hence, a sperm cell swimming along a helical path will directly head for a target releasing chemoattractant once the helix axis has aligned with the concentration gradient. This behavior is quite different from the case of planar chemotaxis along a circular path where the drift speed of sperm swimming circles toward a target is always proportional to the strength of the gradient. Thus sperm chemotaxis in three-dimensional space along helical paths is more efficient than along circular paths in a plane close to a boundary surface. In a forthcoming publication, we will extend the stochastic description of sperm chemotaxis presented here for planar swimming paths to the case of helical swimming paths in three-dimensional space.

In summary, we conclude that the circular and helical swimming paths of sea urchin sperm cells provide an effective means of sampling the local chemoattractant concentration field and detecting a concentration gradient. Whether noise can enhance sperm–egg encounter rates remains an interesting but nontrivial question [31, 32].

Acknowledgments

We thank U B Kaupp and B Lindner for stimulating discussions. This work was funded by the Max-Planck society. BMF acknowledges a scholarship from the German National Academic Foundation.

Appendix A. Coarse-grained description for the centerline

We derive a coarse-grained description of the centerline of stochastic swimming paths. We restrict ourselves to the limit case of weak noise as specified in section 3.3. We introduce a discrete centerline $\hat{\underline{\mathrm{R}}}(t_k)$ which is defined for the discrete times $t_k = k\,\Delta t$, $k = 0, 1, 2, \ldots$, and which has the same drift and variance as $\underline{\mathrm{R}}(t_k)$ to leading order in η and ν. The stochastic process generating $\hat{\underline{\mathrm{R}}}(t_k)$ is defined by the following stochastic difference equation:

$$\hat{\underline{\mathrm{R}}}(t_{k+1}) = \hat{\underline{\mathrm{R}}}(t_k) - \mathrm{i}\, v_\mathrm{d}\, \mathrm{e}^{-\varphi_k}\, \Delta t + \underline{\Xi}_k. \tag{A.1}$$

Here $\underline{\Xi}_k$ is a complex random variable with mean zero. In view of (3.21) and (3.23), the second moments of $\underline{\Xi}_k$ are given by

$$\langle |\underline{\Xi}_k|^2 \rangle = 4D\,\Delta t \quad \text{and} \quad \langle \underline{\Xi}_k^2 \rangle = 0. \tag{A.2}$$

Note that $v_d = v_d(c)$ and $D = D(c)$ depend on concentration and should be evaluated with $c = c(\underline{R}(t_k))$ for the kth time step. If we choose $\Delta t = nT$ longer than the correlation time of total curvature fluctuations $\xi_\kappa(t)$, we may treat the stochastic increments $\underline{\Xi}_k$ in equation (A.1) for different k as mutually independent. Now equation (A.1) describes an Euler scheme for the numerical integration of a stochastic differential equation in the Itō interpretation. We can perform the continuum limit of (A.1) and obtain the stochastic differential equation (4.1) for the continuous-time stochastic path $\hat{\underline{R}}(t)$.

Appendix B. Equation of motion in a radial concentration field

In this appendix, we derive the Itō stochastic differential equation (5.1) which describes coarse-grained sperm swimming paths in a radial concentration field of chemoattractant. Recall that the rules of the Itō stochastic calculus differ from the usual rules of ordinary calculus: suppose that $x_k(t)$, $k = 1, \ldots, n$, is a solution to the set of Itō stochastic differential equations $\dot{x}_k = h_k + g_{kl}\xi_l$ where ξ_l is Gaussian white noise with $\langle \xi_k(t_1)\, \xi_l(t_2)\rangle = \delta_{kl}\, \delta(t_1 - t_2)$ and we use Einstein summation convention. If $y = y(x_k)$ is a function of the x_k, then the Itō chain rule holds [17]

$$\dot{y} = \frac{\partial y}{\partial x_j}\dot{x}_j + \frac{1}{2}\frac{\partial^2 y}{\partial x_k \partial x_l} g_{km} g_{ml}. \tag{B.1}$$

Equation (4.1) describes the stochastic dynamics of R_1 and R_2 with $\underline{R} = R_1 + \mathrm{i}R_2$. For the dynamics of $R = \sqrt{R_1^2 + R_2^2}$ and $\psi = \arctan(R_2/R_1)$, we find using the Itō chain rule (B.1)

$$\begin{aligned} \dot{R} &= -v_d \cos\alpha + \xi_1 \cos\psi + \xi_2 \sin\psi + D/R, \\ \dot{\psi} &= (-v_d \sin\alpha - \xi_1 \sin\psi + \xi_2 \cos\psi)/R. \end{aligned} \tag{B.2}$$

The equation for $\dot{R}$ contains a noise-induced drift term D/R due to the rules of Itō stochastic calculus. We introduce $\xi_1' = \xi_1 \cos\psi + \xi_2 \sin\psi$ and $\xi_2' = -\xi_1 \sin\psi + \xi_2 \cos\psi$. Since ξ_j and ψ are independent in the Itō calculus, we conclude that ξ_j' are again Gaussian white noise terms with $\langle \xi_k'(t_1)\xi_2'(t_2)\rangle = 2D\, \delta_{kl}\delta(t_1 - t_2)$. Hence, the stochastic dynamics of R and ψ can equivalently be described by equation (5.1).

References

[1] Böhmer M, Van Q, Weyand I, Hagen V, Beyermann M, Matsumoto M, Hoshi M, Hildebrand E and Kaupp U B 2005 Ca^{2+}-spikes in the flagellum control chemotactic behaviour of sperm *EMBO J.* **24** 2741–52

[2] Eisenbach M and Giojalas L C 2006 Sperm guidance in mammals—an unpaved road to the egg *Nat. Rev. Mol. Cell Biol.* **7** 276–85

[3] Gray J 1955 The movement of sea-urchin spermatozoa *J. Exp. Biol.* **32** 775–801

[4] Kaupp U B, Solzin J, Hildebrand E, Brown J E, Helbig A, Hagen V, Beyermann M, Pampaloni F and Weyand I 2003 The signal flow and motor response controling chemotaxis of sea urchin sperm *Nat. Cell Biol.* **5** 109–17

[5] Strünker T, Weyand I, Bönigk W, Van Q, Loogen A, Brown J E, Kashikar N, Hagen V, Krause E and Kaupp U B 2006 A K^+-selective cGMP-gated ion channel controls chemosensation of sperm *Nat. Cell Biol.* **8** 1149–54

[6] Brokaw C J 1979 Calcium-induced asymmetrical beating of triton-demembranated sea urchin sperm flagella *J. Cell Biol.* **82** 401–11

[7] Kaupp U B, Kashikar N D and Weyand I 2008 Mechanisms of sperm chemotaxis *Annu. Rev. Physiol.* **70** 93–117
[8] Miller R L 1985 Sperm chemo-orientation in the metazoa *Biology of Fertilization* vol 2 *Biology of the Sperm* ed C B Metz and A Monroy (New York: Academic) pp 275–337
[9] Yoshida M, Ishikawa M, Izumi H, De Santis R and Morisawa M 2003 Store-operated calcium channel regulates the chemotactic behavior of ascidian sperm *Proc. Natl Acad. Sci. USA* **100** 149–54
[10] Wood C D, Nishigaki T, Furuta T, Baba A S and Darszon A 2005 Real-time analysis of the role of Ca^{2+} in flagellar movement and motility in single sea urchin sperm *J. Cell Biol.* **169** 725–31
[11] Kaupp U B, Hildebrand E and Weyand I 2006 Sperm chemotaxis in marine invertebrates—molecules and mechanisms *J. Cell. Phys.* **208** 487–94
[12] Friedrich B M and Jülicher F 2007 Chemotaxis of sperm cells *Proc. Natl Acad. Sci. USA* **104** 13256–61
[13] Barkai N and Leibler S 1997 Robustness in simple biochemical networks *Nature* **387** 913–7
[14] Alon U, Surette M G, Barkai N and Leibler S 1999 Robustness in chemical networks *Nature* **397** 168–71
[15] Sendiña-Nadal I, Alonso S, Pérez-Muñuzuri V, Gómez-Gesteira M, Pérez-Villar V, Ramírez-Piscina L, Casademunt J, Sancho J M and Sagués F 2000 Brownian motion of spiral waves driven by spatiotemporal structured noise *Phys. Rev. Lett.* **84** 2734–7
[16] van Teeffelen S and Löwen H 2008 Dynamics of a Brownian circle swimmer *Phys. Rev.* E **78** 020101
[17] Øksendal B 2000 *Stochastic Differential Equations* (Berlin: Springer)
[18] Lau A W C and Lubensky T C 2007 State-dependent diffusion: thermodynamic consistency and its path integral formulation *Phys. Rev.* E **76** 011123
[19] Risken H 1996 *The Fokker–Planck Equation* (Berlin: Springer)
[20] Alt W and Schaaf R 1985 Chemotaxis of gametes: a diffusion approximation *IMA J. Math. Appl. Med. Biol.* **2** 109–29
[21] Riedel-Kruse I H, Hilfinger A, Howard J and Jülicher F 2007 How molecular motors shape the flagellar beat *HFSP* **1** 192–208
[22] Farley G S and Levitan D R 2001 The role of jelly coats in sperm–egg encounters, fertilization success, and selection on egg size in broadcast spawners *Am. Naturalist* **157** 626–36
[23] Riedel I H, Kruse K and Howard J 2005 A self-organized vortex array of hydrodynamically entrained sperm cells *Science* 300–3
[24] Berg H C and Brown D A 1972 Chemotaxis in *Escherichia coli* analysed by three-dimensional tracking *Nature* **239** 500–4
[25] Segall J E, Block S M and Berg H C 1986 Temporal comparisons in bacterial chemotaxis *Proc. Natl. Acad. Sci. USA* **83** 8987–91
[26] Crenshaw H C 1996 A new look at locomotion in microorganisms: rotating and translating *Am. Zool.* **36** 608–18
[27] Corkidi G, Taboada B, Wood C D, Guerrero A and Darszon A 2008 Tracking sperm in three-dimensions *Biochem. Biophys. Res. Commun.* **373** 125–9
[28] Hilfinger A and Jülicher F 2008 The chirality of ciliary beats *Phys. Biol.* **5** 016003
[29] Elgeti J and Gompper G 2008 Hydrodynamics of active mesoscopic systems *NIC Symp. 2008* vol 39 ed G Münster, D Wolf and M Kremer (Jülich: John von Neumann Institute for Computing) pp 53–62
[30] Brokaw C J 1958 Chemotaxis of bracken spermatozoids *J. Exp. Biol.* **35** 197–212
[31] Friedrich B M 2008 Search along persistent random walks *Phys. Biol.* **5** 026007
[32] Riffell J A and Zimmer R K 2007 Sex and flow: the consequences of fluid shear for sperm–egg interactions *J. Exp. Biol.* **210** 3644–60